Materials Reports: Energy 5 (2025) 100311

Contents lists available at ScienceDirect

Materials Reports: Energy

journal homepage: www.keaipublishing.com/en/journals/materials-reports-energy

Original Research Report

Polymerized-ionic-liquid-based solid polymer electrolyte for ultra-stable lithium metal batteries enabled by structural design of monomer and crosslinked 3D network

Lingwang Liu [a,b,1], Jiangyan Xue [b,1], Yiwen Gao [b,c], Shiqi Zhang [b], Haiyang Zhang [b], Keyang Peng [a,b], Xin Zhang [a,b], Suwan Lu [a,b], Shixiao Weng [a,b], Haifeng Tu [a,b], Yang Liu [a,b], Zhicheng Wang [d,e], Fengrui Zhang [d,e], Daosong Fu [d], Jingjing Xu [f,*], Qun Luo [a,b,**], Xiaodong Wu [a,b,***]

[a] School of Nano-Tech and Nano-Bionics, University of Science and Technology of China, Hefei, 230026, China
[b] i-Lab, Suzhou Institute of Nano-Tech and Nano-Bionics (SINANO), Chinese Academy of Sciences, Suzhou, 215123, China
[c] School of Materials Science and Engineering, Shanghai University, Shanghai, 200444, China
[d] Tianmu Lake Institute of Advanced Energy Storage Technologies, Liyang, 213300, China
[e] Institute of Physics Chinese Academy of Sciences, Beijing, 100190, China
[f] College of Material Science and Engineering, Hohai University, Changzhou, 213022, China

ARTICLE INFO

Keywords:
Polymerized ionic liquid
Solid polymer electrolyte
Structural design
Crosslinked 3D network
Lithium metal battery

ABSTRACT

Solid polymer electrolytes (SPEs) have attracted much attention for their safety, ease of packaging, cost-effectiveness, excellent flexibility and stability. Poly-dioxolane (PDOL) is one of the most promising matrix materials of SPEs due to its remarkable compatibility with lithium metal anodes (LMAs) and suitability for in-situ polymerization. However, poor thermal stability, insufficient ionic conductivity and narrow electrochemical stability window (ESW) hinder its further application in lithium metal batteries (LMBs). To ameliorate these problems, we have successfully synthesized a polymerized-ionic-liquid (PIL) monomer named DIMTFSI by modifying DOL with imidazolium cation coupled with $TFSI^-$ anion, which simultaneously inherits the lipophilicity of DOL, high ionic conductivity of imidazole, and excellent stability of PILs. Then the tridentate crosslinker trimethylolpropane tris[3-(2-methyl-1-aziridine)propionate] (TTMAP) was introduced to regulate the excessive Li^+-O coordination and prepare a flame-retardant SPE (DT-SPE) with prominent thermal stability, wide ESW, high ionic conductivity and abundant Li^+ transference numbers (t_{Li+}). As a result, the $LiFePO_4$|DT-SPE|Li cell exhibits a high initial discharge specific capacity of 149.60 mAh g^{-1} at 0.2C and 30 °C with a capacity retention rate of 98.68% after 500 cycles. This work provides new insights into the structural design of PIL-based electrolytes for long-cycling LMBs with high safety and stability.

1. Introduction

As the current mainstream energy source, secondary lithium (Li)-ion batteries (LIBs) have been widely used in portable electronics and electric vehicles for decades. However, low energy density constrains their future development.[1,2] Li metal batteries (LMBs) with extremely high theoretical specific capacity (3860 mAh g^{-1}) and very low electrochemical potential (−3.04 V versus standard hydrogen electrode) of Li metal anodes (LMAs) are promising to solve the bottleneck problem.[3,4] However, the uneven Li deposition/stripping behavior and uncontrolled growth of Li dendrites pose serious threats to the safety of LMBs. Numerous strategies have been proposed to reduce the risk of failure and improve cycling stability, among which electrolyte engineering takes the lead in terms of research depth and width.[5,6] Solid polymer electrolytes (SPEs)

* Corresponding author.
** Corresponding author. School of Nano-Tech and Nano-Bionics, University of Science and Technology of China, Hefei, 230026, China.
*** Corresponding author. School of Nano-Tech and Nano-Bionics, University of Science and Technology of China, Hefei, 230026, China.
E-mail addresses: jjxu2011@sinano.ac.cn (J. Xu), qluo2011@sinano.ac.cn (Q. Luo), xdwu2011@sinano.ac.cn (X. Wu).
[1] Lingwang Liu and Jiangyan Xue contributed equally to this work.

https://doi.org/10.1016/j.matre.2024.100311
Received 26 September 2024; Received in revised form 8 December 2024; Accepted 8 December 2024
Available online 30 December 2024

are promising alternatives to traditional organic liquid electrolytes that can increase the safety and energy density of LMBs.[7–9] Among various SPEs, polymerized-ionic-liquid (PIL)-based SPEs not only possess the high flexibility of polymers but also inherit the satisfactory stability and safety of ionic liquids, which enable improved electrolyte/electrode interface contact together with good cycling performance.[3,10]

1,3-Dioxolane (DOL) has been extensively studied in polymer electrolytes due to its good compatibility with LMAs, which can undergo cationic polymerization in the presence of Lewis acids. However, linear poly-dioxolane (PDOL)-based SPEs remain some notable defects, such as poor thermal stability, insufficient ionic conductivity and narrow electrochemical stability window (ESW). Plenty of strategies have been proposed to address these issues, such as introducing poly(ethylene glycol)-SiO_2 hairy nanoparticles to boost the ion-transport properties,[11] or designing a hybrid polymer-alloy-fluoride interphase embedded in the PDOL matrix on the Li surface (Li-Ag/LiF) to improve the electrochemical reaction kinetics,[12] or increasing the alkyl chain length by changing DOL to a six-membered ring ether 1,3-dioxane (DOX) to enhance oxidative stability and promote the formation of an anion-derived, inorganic-rich solid electrolyte interphase (SEI).[13] Nevertheless, the challenge remains in how to improve the thermal and electrochemical stability of PDOL-based SPEs while maintaining excellent ionic conductivity and interface compatibility.

Herein, we developed a flame-retardant DT-SPE through the design of the monomer's molecular structure and the construction of a crosslinked 3D network to achieve excellent ionic conductivity as well as thermal and electrochemical stability. First, the DOL-based PIL monomer (denoted as DIMTFSI) was designed and successfully synthesized by adding an imidazolium cation to DOL and loading $TFSI^-$ through anion exchange. Afterward, PDIMTFSI-SPE was prepared by selecting lithium bis(trifluoromethanesulfonyl)imide (LiTFSI) as salt followed by a cationic ring-opening polymerization in the presence of the Lewis acid initiator tris(pentafluorophenyl)borane (TPFPB). The structural design of DIMTFSI monomer endows the PDIMTFSI-SPE with a cationic backbone that promotes the dissociation of LiTFSI, as well as sufficient thermal stability and rigorous non-flammability. Then, in order to alleviate the side effects of excessive Li^+-O coordination in PDIMTFSI-SPE, crosslinker trimethylolpropane tris[3-(2-methyl-1-aziridine) propionate] (TTMAP) was introduced to incorporate with PDIMTFSI to prepare DT-SPE. The functions of the tridentate crosslinker TTMAP are concluded as the following aspects: (1) reducing the content of active hydroxyl groups in the bulk phase and broadening the ESW (4.3 V); (2) weakening the coordination between Li^+ and the oxygen atoms of ether groups from polymer chains, promoting Li^+ transference number (0.31) and ambient ionic conductivity (4.6×10^{-4} S cm^{-1}); (3) converting linear structure to 3D network and enhancing the stability of SPEs. Benefiting from the cooperative influence between the design of molecular structure and the construction of a crosslinked 3D network, the Li|DT-SPE|Li symmetric cell enables reversible and stable Li deposition/stripping for over 1000 h under 0.1 mA cm^{-2} with 0.1 mAh cm^{-2} per half cycle. Furthermore, the $LiFePO_4$|DT-SPE|Li cell manifests high initial discharge capacity (149.60 mAh g^{-1}) and capacity retention (98.68%) after 500 cycles at 0.2C under 30 °C. This work provides new guidance for the design of SPEs with both prominent stability and safety, paving the way for achieving the long-cycle performance of LMBs.

2. Experimental section

2.1. Materials

2-Chloromethyl-1,3-dioxolane (>98%, Alfa Aesar), N-methylimidazole (99%, Adamas), trimethylolpropane tris[3-(2-methyl-1-aziridine) propionate] (TTMAP) (99%, Adamas), ethyl acetate (99%, Aladdin), tris(pentafluorophenyl)borane (TPFPB) (97%, Adamas), trichloromethane (AR, Sinopharm), and anhydrous ethanol (99%, Aladdin) were used without any processing. Dimethoxyethane (DME) (>98%, Adamas) was soaked in 3A molecular sieve for 24 h before use. Lithium bis(trifluoromethanesulfonyl)imide (LiTFSI) was purchased from Aladdin, and glass fiber/A (GF/A) from Whatman, both of which were dried at 80 °C under vacuum for 24 h.

2.2. Synthesis of 3-(1,3-dioxolan-2-ylmethyl)-1-methylimidazolium chloride and 3-(1,3-dioxolan-2-ylmethyl)-1-methylimidazolium bis(trifluoromethanesulfonyl)-imide

3-(1,3-dioxolan-2-ylmethyl)-1-methylimidazolium chloride (DIMCl) was synthesized via a one-step addition reaction: 57.14 g of 2-chloromethyl-1,3-dioxolane and 39.34 g of N-methylimidazole were added to 21.34 g of chloroform. The solution was heated at 90 °C for 48 h under reflux condensation. Afterward, the remaining solvent was removed by vacuum distillation at 40 °C. Subsequently, ethyl acetate was added for liquid separation and the process was repeated three times to ensure the complete removal of the reactants.

3-(1,3-dioxolan-2-ylmethyl)-1-methylimidazolium bis(trifluoromethanesulfonyl)imide (DIMTFSI) was obtained through anion exchange: 30.00 g of LiTFSI was dissolved in 20 mL deionized water and the solution was added dropwise into the DIMCl solution, followed by stirring for 12 h to ensure sufficient anion exchange. Deionized water was then used as the solvent to perform the liquid separation process three times to remove excess LiTFSI. Due to the stringent requirements on water content for subsequent applications in LMBs, freeze-drying and immersion of molecular sieves in a glovebox with $O_2 < 1$ ppm, and $H_2O < 1$ ppm were carried out successively after the liquid separation for the maximum extent of water removal.

2.3. Preparation of electrode and solid polymer electrolytes

First, we prepared a slurry containing $LiFePO_4$ (LFP), acetylene black and poly(vinylidene difluoride) in a weight ratio of 8:1:1 using N-methyl-2-pyrrolidone (NMP) as the solvent. Then the slurry was coated onto Al foil to obtain LFP cathode. The cathode plate was dried in the vacuum oven at 80 °C overnight and the loading of active substance mass of the as-prepared 12 mm diameter cathode is 2.30 mg cm^{-2}.

The polymer electrolyte precursor was prepared by dissolving 1 M LiTFSI in DIMTFSI monomer along with 5 wt% TTMAP and 1 wt% TPFPB in the presence of trace amounts of DME. After magnetic stirring for 30 min, 50 μL precursor solution was absorbed to coat the surface of the cathode. Then a GF/A supporter with a diameter of 19 mm was covered on it and another 50 μL precursor solution was added onto the supporter. After that, the cathode with precursor was kept in the vacuum oven overnight at room temperature to remove DME and perform the polymerization. Eventually, the anode was placed onto the SPE and then encapsulated.

The degree of polymerization is mainly controlled in three aspects: the amount of initiator and crosslinker as well as the time of cationic polymerization. For a balanced comprehensive performance, we maintained the initiator TPFPB and crosslinker TTMAP at 1 wt% and 5 wt% of the DIMTFSI monomer, respectively. The polymerization time was set to 12 h under vacuum conditions in this study.

The comparison sample PDIMTFSI-SPE was prepared using the same steps as above, but without the addition of crosslinker TTMAP.

2.4. Characterization

Fourier Transform Infrared Spectroscopy (FT-IR) was obtained by Thermo Fisher Scientific Nicolet 6700 spectrometer equipped with an ATR accessory and ^1H, ^{13}C Nuclear Magnetic Resonance (NMR) was conducted on a Varian 400 MHz spectrometer to elucidate the chemical structures of both monomers and polymers. Using the NETZSCH differential scanning calorimetry (DSC) instrument (200 F3 Maia), DSC was performed over a temperature range of −100–20 °C under a N_2 atmosphere, with a heating rate set at 10 °C per minute. In order to assess the

thermal properties of the SPEs, thermogravimetric analysis (TGA) was conducted on the TG/DTA6300 instrument from 30 °C to 500 °C at a heating rate of 10 °C per minute under a N_2 atmosphere. The field emission scanning electron microscope (SEM) was carried out by Hitachi S-4800 to characterize the morphologies of the SPEs. X-ray photoelectron spectroscopy (XPS) analysis was conducted on the ESCALAB 250Xi spectrometer (VG, Altrincham) employing Al Kα radiation as the excitation source. The instrument model of gel permeation chromatography (GPC) is Agilent 1260 with tetrahydrofuran (THF) serving as the mobile phase and using polystyrene (PS) as the reference standard under 35 °C.

The samples underwent a cleaning process with DME in the glovebox and then dried in a vacuum oven for 3 h to ensure complete evaporation of any residual solvent. Subsequently, the samples were transferred to the XPS analysis chamber using a vacuum transfer apparatus, thereby preventing any exposure to air or moisture. To assess the non-flammability of the SPEs on the support, a plastic ignition gun was utilized to create a flame, and the SPEs were held in place for 3–5 s.

2.5. Electrochemical characterization

All of the electrochemical measurements were performed employing CR2032 coin cells. The ionic conductivities (σ) of the SPEs were quantified through alternating current (AC) impedance spectroscopy, conducted on an electrochemical workstation (Bio-logic, VPM-300) at various temperatures ranging from 30 °C to 80 °C. The spectra were recorded across the frequency range spanning from 7 MHz to 500 MHz, with the SPEs positioned between two stainless steels (SS) that served as blocking electrodes. According to Equation (1), the ionic conductivities of SPEs could be calculated.[14]

$$\sigma = \frac{d}{RS} \tag{1}$$

The thickness of the electrolyte film is denoted by d, while the electrolyte resistance is represented by R, and the effective surface area of the electrode is signified by S. The equation for calculating the activation energy (E_a) based on the Arrhenius formula is shown in Equation (2).

$$\sigma(T) = A \exp\left(-\frac{E_a}{RT}\right) \tag{2}$$

The ionic conductivity of the electrolyte is denoted by σ, the frequency factor is represented by A, the molar gas constant is labeled as R, and the absolute temperature in Kelvin is signified by T.

The Li^+ transference number (t_{Li+}) of the SPEs was measured in Li||Li cells, both the pristine and steady-state current flowing, as well as the alternating current (AC) impedances of the cells were evaluated before and after polarizing at 10 mV for 1 h. Then we select the Bruce-Vincent method to calculate the final value of t_{Li+} according to Equation (3).

$$t_{Li^+} = \frac{I_s(\Delta V - I_0 R_0)}{I_0(\Delta V - I_s R_s)} \tag{3}$$

where I_0 and I_s are the current measured under pristine and steady-state, R_0 and R_s are the impedances measured under pristine and steady-state, ΔV is the applied polarization voltage.

The ESW was characterized by linear sweep voltammetry (LSV) using Li||SS cells on Biologic VPM-300 electrochemical workstation with the voltage going from the open circuit voltage to 6.0 V, and the scan rate was set as 0.1 mV s^{-1}.

The performances of LFP|SPE|Li cells under high-temperature conditions were evaluated in an electrothermal blowing-dry oven (DHG-9070A, Shanghai Jinghong Test Equipment Co., Ltd) undergoing cycling at 0.2C within 2.5 and 4.0 V at corresponding temperatures. The activation process for all of the cells was performed by cycling at 0.1C for 5 periods under 30 °C.

2.6. Theoretical simulations

Molecular dynamics simulations were performed using the Forcite package in the Materials Studio. PDIMTFSI was defined as the polymer segment consisting of 10 DIMTFSI units through homopolymerization. Amorphous cells with the linear dimensions of 33.2 Å and 33.8 Å were adopted, corresponding to the LiTFSI/DIMTFSI/TTMAP molar ratios of 1:33.3:0 for PDIMTFSI-SPE and 1:33.3:1.7 for DT-SPE, respectively. A temporal increment of 1.0 fs was selected and statistical averages were derived from trajectories spanning a minimum of 20 ps in duration after the 5 ps equilibration steps. The NVT ensemble alongside the COMPASS force field was selected to employ, and temperature regulation was achieved through a Nosé thermostat, aiming to maintain a temperature of 298 K.[15] The radial distribution function was calculated by using Equation (4):

$$g(r) = \frac{1}{4\pi r^2 \rho}\frac{dn(r)}{dr} \tag{4}$$

r denotes the distance between species and the target Li^+, ρ signifies the mean probability density of Li^+ dispersed within the electrolyte, dr corresponds to the thickness measured for the spherical shell, while dn(r) represents the count of particles encompassed within that shell.

The CN of species positioned in proximity to the central Li^+ were derived by integrating $g(r)$ with respect to the variable r in Equation (5).

$$CN = 4\pi\rho \int_0^r r^2 g(r)\mathrm{d}r \tag{5}$$

3. Results and discussion

The synthesis process of the DIMTFSI monomer is shown in Fig. 1a, which contains two steps: (1) addition reaction and (2) anion exchange. The addition mechanism is that the lone pair of electrons in the N atom of N-methylimidazole attacks the C atom in the methyl group from 2-chloromethyl-1,3-dioxolane, resulting in the formation of a new C-N^+ bond. Then the anion exchange occurs between Cl^- and $TFSI^-$. In order to verify the successful design of DIMTFSI, FT-IR was used to characterize the functional groups of the mixture of 2-chloromethyl-1,3-dioxolane and N-methylimidazole as well as DIMTFSI monomer (Fig. 1b). In addition to the C-N characteristic vibration peak at 1132 cm^{-1} and C=C characteristic vibration peak at 1475 cm^{-1} of N-methylimidazole, a new C-N^+ stretching vibration peak at 1330 cm^{-1} arises, which corresponds to the successful addition reaction.[16] Furthermore, the vibration peaks of C-F and O=S=O from $TFSI^-$ at 1175 and 1348 cm^{-1} can also be observed, indicating the successful exchange of $TFSI^-$ with Cl^-.[17] The chemical structure of DIMTFSI was also analyzed by ^1H NMR spectrum and the result shows that the structure of the obtained product is in good agreement with the designed structure (Fig. 1c). The results of FT-IR and ^1H NMR demonstrate that the DIMTFSI with high purity can be successfully prepared by the designed synthesis route.

In step (3) of Fig. 1a, DIMTFSI undergoes cationic polymerization with the addition of 1 wt% initiator TPFPB to obtain the homopolymer PDIMTFSI. The boron atoms of TPFPB provide Lewis acidic sites to initiate ring-opening polymerization of DIMTFSI. This can be demonstrated in the ^{13}C NMR spectrum of DIMTFSI and PDIMTFSI in Fig. 1d that except for the original carbon atoms a and b on DIMTFSI monomers at chemical shifts of 99.6 and 65.3 ppm, new peaks of a' and b' on PDIMTFSI appear at 57.8 and 71.6 ppm, indicating the successful ring-opening polymerization of cyclic ethers on DIMTFSI.[18] To make clear the polymer degree of PDIMTFSI, gel permeation chromatography (GPC) was selected to characterize the molecular weight of the PDIMTFSI (Fig. S1). The results, summarized in Table S1, indicate that the polymer chains in PDIMTFSI are relatively short, primarily due to the significant steric hindrance of the DOL ring-opening sites on the monomer, which enables cationic polymerization but only allows the formation of an

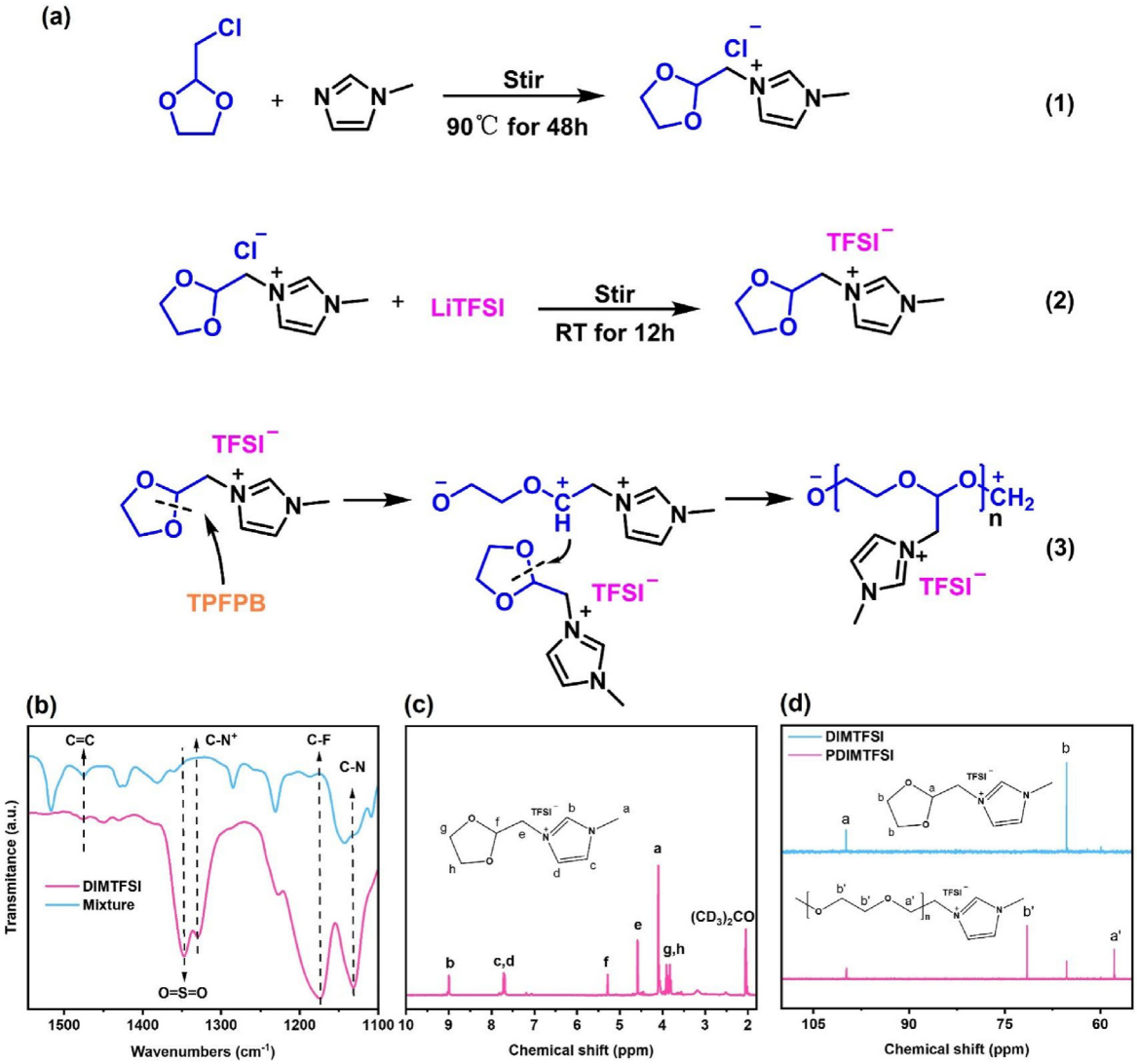

Fig. 1. (a) Synthesis route and polymerization diagram of DIMTFSI. (b) FT-IR spectrum of the mixture and DIMTFSI. (c) ^{1}H NMR spectrum of DIMTFSI. (d) ^{13}C NMR spectra of DIMTFSI before and after polymerization.

oligomer system predominantly composed of dimers or trimers. To enhance the mechanical stability of the polymer, the DIMTFSI monomer was crosslinked to obtain DT-SPE by adding 5 wt% multifunctional crosslinker TTMAP, which has three aziridine terminal groups, into the DIMTFSI precursor solution. The crosslinking mechanism is shown in Fig. S2. Due to the lone pair electrons on the nitrogen atom, the aziridine in TTMAP as the nucleophilic reagent attacked the carbenium ion in the PDIMTFSI to form a new C-N bond. Then the resulting carbenium ion caused by the ring opening of aziridine was captured by another PDIMTFSI, leading to the crosslinked 3D network polymer structures. The FT-IR result in Fig. S3 shows that the intensity of the chain vibration peak for PDIMTFSI, originally located near 840 cm^{-1}, significantly decreases after the addition of a crosslinker. This indicates a reduction in the linear homopolymer PDIMTFSI content and confirms successful crosslinking with TTMAP.[1] The EIS of different stainless steel (SS) symmetrical cells with PDIMTFSI and DT-SPE membranes were carried out to screen for the optimal proportion of LiTFSI and crosslinker in DT-SPE. According to Fig. S4a, the EIS result reaches the smallest value when the optimal concentration of LiTFSI is 1 M. Besides, when the content of TTMAP is 5 wt%, the bulk impedance of DT-SPE reaches the lowest value (36 Ω) in Fig. S4b and the ambient ionic conductivity can be calculated to be 4.6 × 10^{-4} S cm^{-1} according to Equation (1), which is superior to other samples. The optimal concentration of LiTFSI and TTMAP was used to prepare the following PDIMTFSI and DT-SPE membranes.

The effect of structural design and crosslinked 3D network on the electrochemical performance was also evaluated. The LSV results shown in Fig. 2a exhibit that the electrochemical oxidation of PDIMTFSI begins at 4.0 V, while the ESW of DT-SPE increases to approximately 4.3 V. This is mainly due to the positively charged methyl group on the opened aziridine of TTMAP, which initiates the ring-opening polymerization of DIMTFSI, forming a crosslinked polymer chain. This reduces the amount of linear polymer chains containing ether-oxygen bonds with poor electrochemical stability. SS|PDIMTFSI-SPE|SS and SS|DT-SPE|SS symmetric cells were tested for EIS at various temperatures (Fig. S5). The ionic conductivities of PDIMTFSI-SPE and DT-SPE ranging from 30 °C to 80 °C were calculated according to Equation (1) and the results were presented in Fig. 2b and Tables S2–3. Apparently, the DT-SPE shows higher ionic conductivity than PDIMTFSI-SPE across the temperature range from 30 °C to 80 °C, indicating that the transport kinetics of Li^+ in DT-SPE has been enhanced following the formation of crosslinked structure. The activation energy (E_a) of Li^+ was calculated according to the Arrhenius formula (Equation (2)) to be 0.63 eV for PDIMTFSI-SPE and 0.38 eV for DT-SPE. That is to say, the transport barrier of Li^+ in DT-SPE can be maintained at a lower level than that in PDIMTFSI-SPE. This can be attributed to the introduction of plentiful polar ester and amino groups in the crosslinked polymer chain facilitates the dissociation of LiTFSI salt as

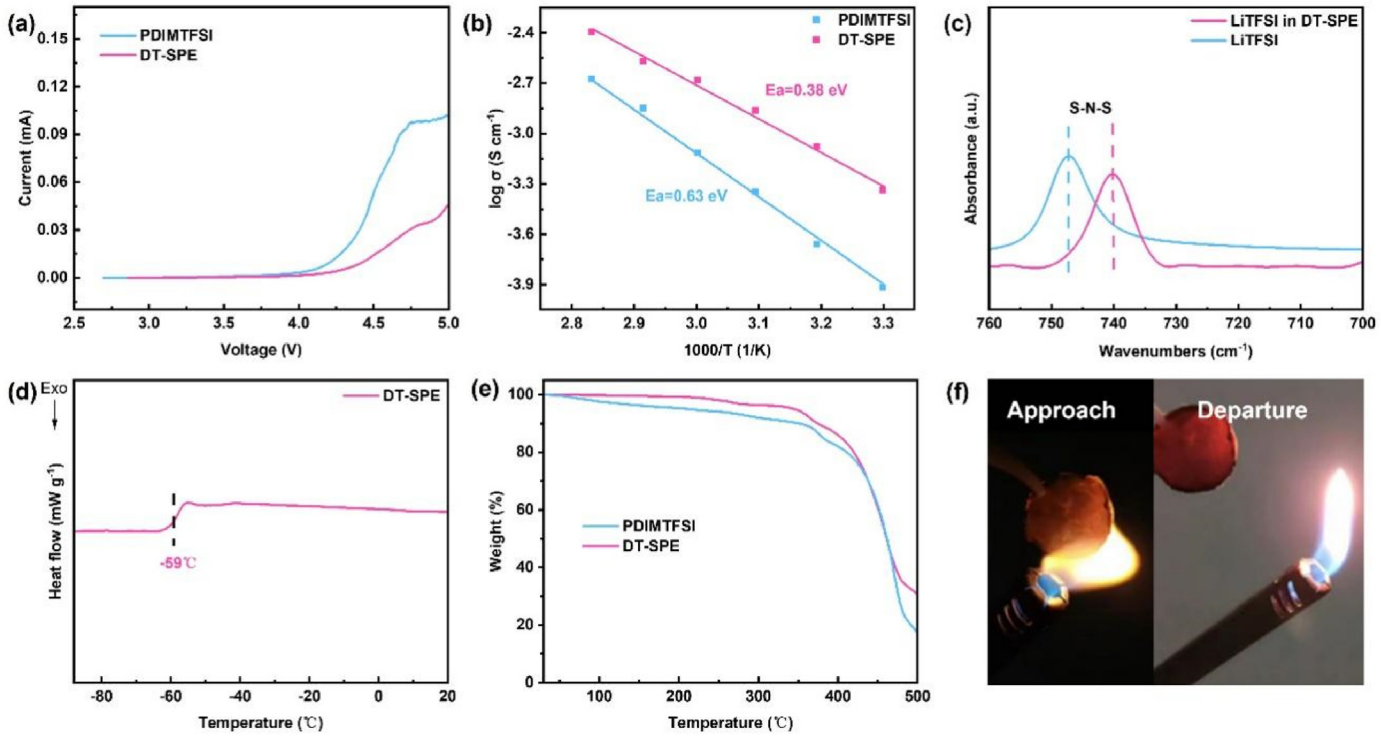

Fig. 2. (a) LSV curves of the Li||SS cells assembled by PDIMTFSI-SPE and DT-SPE at 0.1 mV s^{-1}. (b) Ionic conductivity of PDIMTFSI-SPE and DT-SPE as a function of temperature ranges from 30 °C to 80 °C. (c) FT-IR of pure LiTFSI and DT-SPE. (d) DSC analysis result of DT-SPE. (e) TGA curves of PDIMFSI-SPE and DT-SPE. (f) Combustion experiment of DT-SPE loaded on GF/A supporter.

well as fastens the ionic transport in DT-SPE by weakening the excessive Li^+-O coordination.

In order to explore the reason why DT-SPE exhibits such a high ambient ionic conductivity, the interaction between LiTFSI and DT-SPE was characterized by FT-IR. Fig. 2c manifests that the intrinsic stretching vibration peak of S-N-S in LiTFSI located at 747.3 cm^{-1} shifts to a lower wavenumber (740.2 cm^{-1}) in DT-SPE, indicating that the coordination between Li^+-$TFSI^-$ is weakened.[19] In addition to dissociated Li^+, the ionic conductivity of SPEs is also closely related to the transport of chain segments. Differential scanning calorimetry (DSC) analysis result of DT-SPE in Fig. 2d shows that no phase transition occurs from −90 °C to 20 °C except a glass transition temperature (T_g) at −59 °C, indicating the presence of abundant amorphous regions at room temperature. This is beneficial for the movement of polymer chain segments, which positively contribute to the improved ionic conductivity of DT-SPE.

Thermal stability is a pivotal parameter for SPEs, as it underscores the permissible operating temperature range of batteries and significantly impacts their safety performance. TGA curves in Fig. 2e manifest that the designed monomer endows the PDIMTFSI-SPE with good high-temperature stability which maintains a constant weight within 350 °C and the thermal stability of DT-SPE is not deteriorated after crosslinking with TTMAP owing to the intrinsic thermal stability of crosslinker. In the subsequent ignition test, DT-SPE loaded on GF/A supporter was exposed to the flame for 3 s and no combustion or deformation was observed (Fig. 2f and **Video S1**), indicating its prominent non-flammability and thermostability. In contrast, the PDOL loaded on GF/A exhibited rapid combustion upon contact with the flame and left an obvious black mark on the supporter (Fig. S6 and **Video S2**). In conclusion, DT-SPE exhibits significant improvement in terms of thermal stability and non-flammability compared to previously reported PDOL-SPEs.[2] The structural design of DIMTFSI monomer and construction of crosslinked 3D network not only endow DT-SPE with the inherently excellent thermal stability and non-flammability of both the DIMTFSI and TTMAP units but also ensure good compatibility with LMAs from DOL and ionic liquid components. Additionally, DT-SPE possesses high ionic conductivity from polymer chains with plentiful polar groups and reasonable Li^+-O coordination.

To make clear the reason for fast ionic transport in DT-SPE, Molecular dynamics simulations of PDIMTFSI-SPE and DT-SPE were conducted to study the transfer dynamics of Li^+ and interaction between Li^+ and polymer chains (Fig. 3). The analysis of the radical distribution functions (RDFs, g(r)) and coordination numbers (CNs) for Li^+-O reveals a preference for Li^+ to coordinate with oxygen atoms from $TFSI^-$ anions or the polymer host rather than nitrogen atoms, within their primary solvation shells (Fig. S7). Furthermore, the sharp peaks of g(r) plots at 2.0 Å in Fig. 3b, e vanish as the distance increases, indicating that Li^+ is equipped with a well-defined and ordered coordination sphere in both PDIMTFSI-SPE and DT-SPE.[20] It is noteworthy that the CNs of Li^+-O in PDIMTFSI-SPE are higher than those in DT-SPE, which means that Li^+ ions have stronger coordination with oxygen atoms in PDIMTFSI DT-SPE. For a deeper understanding of the coordination structure of Li^+ in SPEs, atoms in the box within a radius of 3.0 Å were extracted and the results revealed that Li^+ (green balls) in PDIMTFSI-SPE tends to coordinate with five oxygen atoms (red balls) (Fig. 3c), whereas only three oxygen atoms were found around Li^+ in DT-SPE (Fig. 3f). This indicates the Li^+-O coordination in DT-SPE is weaker than that in PDIMTFSI-SPE, which is consistent with the results of aforementioned RDFs and CNs calculations. Benefiting from the weaker Li^+-O coordination, Li^+ transport in DT-SPE is enhanced, leading to a decrease of E_a and an increase of ionic conductivity. In addition to the theoretical calculation results, the t_{Li+} of PDIMTFSI and DT-SPE was calculated according to the chronoamperometry curves and EIS spectra of Li||Li cells via Bruce-Vincent method.[21] Following polarization at 10 mV for 1 h, the t_{Li+} of DT-SPE (0.31) is significantly higher than that of PDIMTFSI-SPE (0.17), demonstrating the promoted Li^+ transport and weakened Li^+-O coordination in DT-SPE (Fig. S8).

Based on the above experimental and molecular dynamics simulation results, the Li^+ ions transport mechanism in PDIMTFSI and DT-SPE is

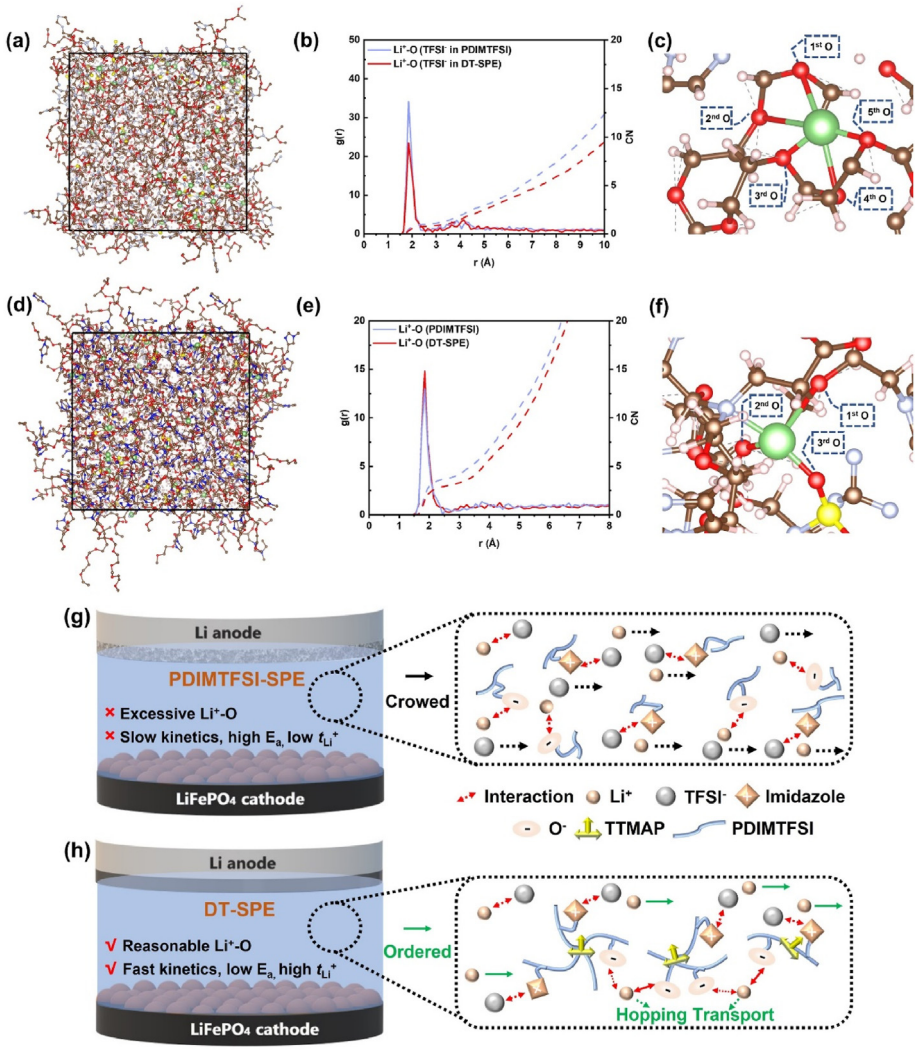

Fig. 3. Molecular dynamics simulation of SPEs: snapshots of (a) PDIMTFSI-SPE and (d) DT-SPE; Radical distribution functions and coordination numbers of Li^+ with oxygen atoms from (b) $TFSI^-$ and (e) polymer chains in PDIMTFSI and DT-SPE; Corresponding coordination structures of Li^+ in (c) PDIMTFSI-SPE and (f) DT-SPE. Schematic illustration of Li^+ transport mechanism in (g) PDIMTFSI-SPE and (h) DT-SPE.

proposed. As shown in Fig. 3g, the existing linear polymer chain with abundant ether-oxygen bonds in PDIMTFSI dissociates LiTFSI and coordinates tightly with Li^+, leading to slow ionic transport. However, due to the incorporation of TTMAP in DT-SPE, the abundant polar groups can further promote the dissociation of LiTFSI, the coordination of Li^+-O from polymer host is weakened and the Li^+ ions can transport by hopping mechanism in the polymer chain. As a result, DT-SPE exhibits faster Li^+ transport kinetics, a lower E_a and a higher t_{Li+} (Fig. 3h).

To investigate the interface compatibility between LMA and DT-SPE, Li|DT-SPE|Li symmetric cells were assembled and subjected to constant-current charge/discharge cycles. The Li|DT-SPE|Li cell exhibits a stable and highly reversible Li plating and stripping for 1000 h with a low overpotential of 0.15 V when tested at 0.1 mA cm^{-2} with 0.1 mAh cm^{-2} per half cycle at 30 °C (Fig. 4a). From Fig. 4b, the surface of LMA in Li|DT-SPE|Li cell shows a smooth and flat morphology without any dendrites. These results conclusively demonstrate that DT-SPE exhibits excellent interfacial stability toward LMAs, enabling long-term stable and reversible Li deposition/stripping, due primarily to the enhanced Li^+ transport facilitated by the weakened Li^+-O coordination and stable interface. Besides, a Li symmetric cell assembled with DT-SPE was used to conduct the rate performance with current density varied from 0.05 mA cm^{-2} to 0.2 mA cm^{-2} (Fig. S9). The overpotentials of the Li|DT-SPE|Li cell remain stable at 0.05, 0.1 and 0.2 mA cm^{-2} with values of 98, 196 and 403 mV, indicating excellent interface stability between DT-SPE and LMAs in the plating/stripping of Li^+ under varied current densities. A critical current density of the symmetric cell based on DT-SPE is 0.46 mA cm^{-2}, which means it can maintain high electrochemical stability under high current densities (Fig. S10).[22]

The chemical composition of SEI on the surface of LMAs in Li|DT-SPE|Li cells, after cycling for 1000 h, was investigated by XPS. The C–F bond (292.8 eV) from $TFSI^-$ as well as C–C (284.5 eV), C–N^+ (286.4 eV), C–O (286.9 eV) and O=C–O (289.1 eV) from DIMTFSI and TTMAP units are observed in the C 1s spectrum (Fig. 4c).[8] The N 1s spectrum in Fig. 4d shows the intrinsic C–N^+, NS=O^- located at 401.9, 399.6 eV and the peak at 399.3 eV can be attributed to Li_3N.[23] Fig. 4e exhibits that the F 1s spectrum consists of three distinct peaks representing LiF, C–F and S–F located at 684.9, 687.6 and 688.6 eV, respectively.[12] The S 2p spectrum in Fig. 4f reveals the peaks located at 187.2 eV (RSO_3Li), 168.9 eV (Li_2SO_3) and 170.1 eV ($LiSO_4$), mostly originating from the reduction of $TFSI^-$.[24] It can be confirmed from the above XPS results that the SEI layer is mainly composed of inorganic components such as LiF, Li_3N, Li_2SO_3, etc., derived from the decomposition of $TFSI^-$. Among them, LiF has been proven to inhibit the continuous decomposition of electrolytes by enhancing the electrochemical inertness of the SEI film, while Li_3N can reduce the interface impedance by promoting the migration of Li^+ in the SEI layer.[25] Additionally, inorganic phases such as Li_2SO_3 can increase

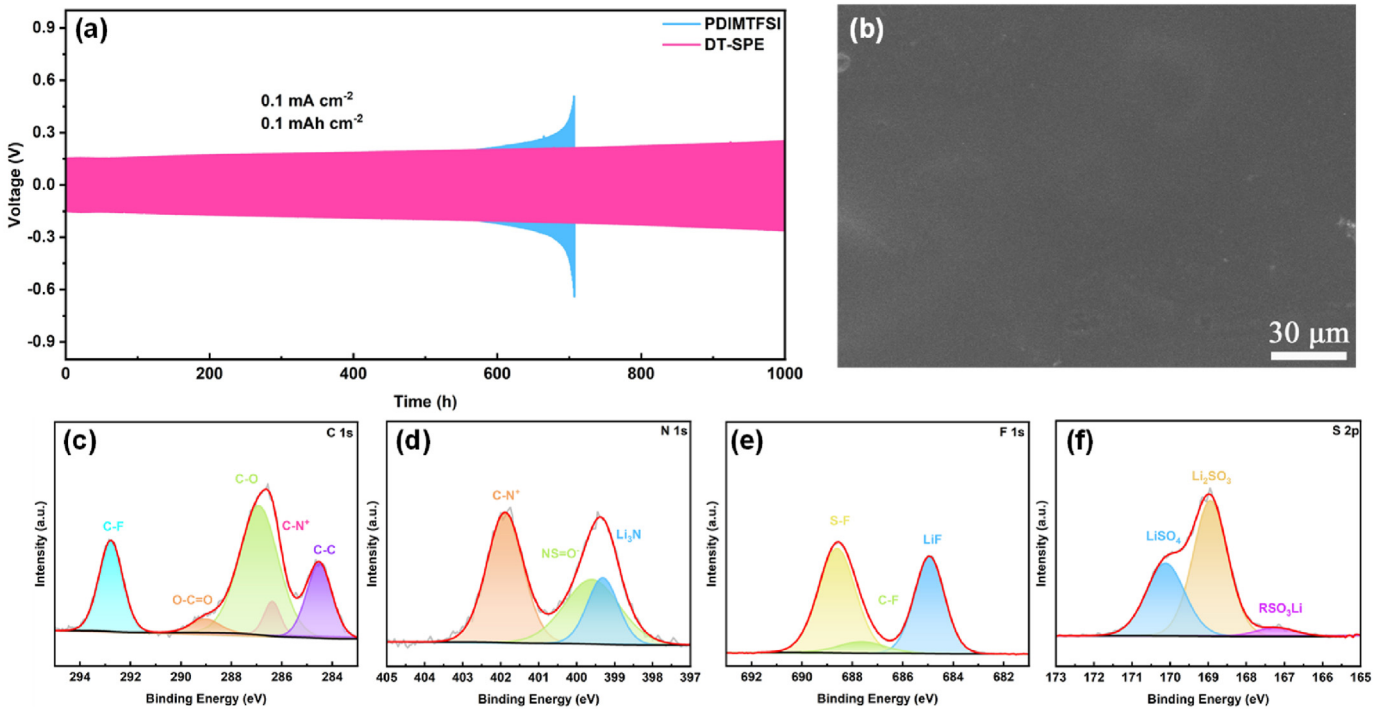

Fig. 4. The voltage-time profiles of (a) Li symmetric cell assembled with DT-SPE at 0.1 mA cm^{-2}, 0.1 mAh cm^{-2} per half cycle. (b) SEM image of cycled LMA disassembled from Li|DT-SPE|Li cell after cycling at 0.1 mA cm^{-2} for 1000 h. XPS spectra of (c) C 1s, (d) N 1s, (e) F 1s and (f) S 2p of LMAs retrieved from Li|DT-SPE|Li cell after 500 cycles.

the shear modulus of the SEI film, inhibiting the growth of Li dendrites by enhancing its mechanical strength.[26] In summary, the designed DT-SPE can facilitate the formation of SEI rich in inorganic components with excellent stability and mechanical strength to inhibit the continuous growth of Li dendrites and maintain good interfacial stability during long-term cycling.

Considering the prominent properties of DT-SPE, we further explore its application in LMBs. As depicted in Fig. 5a, the initial discharge capacity of the LFP|DT-SPE|Li cell at 30 °C and 0.2C is 149.60 mAh g^{-1}, and it maintains a capacity of 147.64 mAh g^{-1} after 500 cycles between 2.5 and 4.0 V with the coulombic efficiency (CE) close to 100%. The capacity retention rate is calculated to be as high as 98.68%. Meanwhile, the LFP|| Li cell assembled with DT-SPE displays good rate-capability, which can be attributed to the optimized Li^+ transport kinetics due to the weak Li^+-O coordination (Fig. S11).[27] The EIS spectra of LFP|DT-SPE|Li before and after 500 cycles combined with the equivalent circuit diagram in Fig. 5b show that the bulk impedance of the cell does not change significantly (from 21.34 Ω to 24.73 Ω) and the SEI impedance only increased slightly, which demonstrates the remarkable compatibility between DT-SPE and LMAs during the continuous Li plating/stripping.

Since DT-SPE possesses an abundant thermal stability window, the long-term cycling performance of LFP|DT-SPE|Li cell at 0.2C under 60 °C

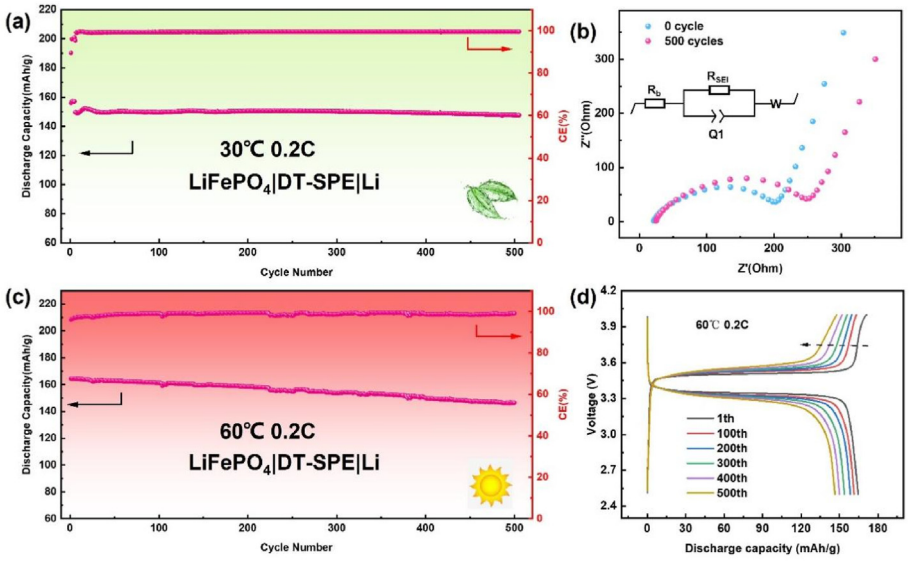

Fig. 5. (a) Evaluation of the cycling performance at 30 °C of the LFP|DT-SPE|Li and (b) EIS spectra of the cell before and after 500 cycles. (c) Cycling performance of the LFP|DT-SPE|Li under 60 °C and (d) charge/discharge characteristic curves of the cell under different cycles.

has also been investigated. The result shows that the discharge specific capacity slowly decreases from 164.49 mAh g^{-1} to 146.41 mAh g^{-1} after 500 cycles and the average CE remains near 99% (Fig. 5c). Moreover, the capacity retention rate of LFP|DT-SPE|Li under 60 °C slightly decreased by 9.81% compared to that at 30 °C, indicating that the side reactions at high temperatures have been effectively inhibited owing to the prominently stable DT-SPE.[3] Besides, no significant increase of polarization has been observed in the galvanostatic charge-discharge curves due to the satisfactory ionic conductivity and excellent interface stability (Fig. 5d).

4. Conclusion

In this work, we successfully proposed a strategy for structural design and the construction of a crosslinked 3D network to modify DOL-based SPEs with excellent physical and chemical properties as well as electrochemical performance. We elucidate the electrochemical enhancement mechanism of the DT-SPE in detail, including ambient ionic conductivity (4.6×10^{-4} S cm^{-1}), broadened wide ESW (4.3 V), decreased E_a (0.38), enhanced t_{Li+} (0.31), improved interfacial stability, as well as rigorous non-flammability. Consequently, the LFP|DT-SPE|Li cell exhibits a high initial discharge capacity of 149.60 mAh g^{-1} at 0.2C, 30 °C with a distinguished capacity retention rate of 98.68% after 500 cycles and prominent interfacial compatibility thanks to the reasonable Li^+-O coordination. It is expected that the monomer structural design and crosslink strategy will broaden the horizon in the development of safe PILs-based SPEs with high performance for LMBs.

CRediT authorship contribution statement

Lingwang Liu: Writing – review & editing, Writing – original draft, Visualization, Validation, Software, Resources, Methodology, Investigation, Formal analysis, Data curation, Conceptualization. **Jiangyan Xue:** Writing – review & editing, Visualization, Supervision, Funding acquisition, Conceptualization. **Yiwen Gao:** Software. **Shiqi Zhang:** Visualization, Methodology. **Haiyang Zhang:** Validation, Resources. **Keyang Peng:** Validation, Data curation. **Xin Zhang:** Validation, Data curation. **Suwan Lu:** Visualization, Investigation. **Shixiao Weng:** Formal analysis, Data curation. **Haifeng Tu:** Supervision, Software, Investigation. **Yang Liu:** Resources, Methodology. **Zhicheng Wang:** Resources, Methodology, Investigation. **Fengrui Zhang:** Supervision, Investigation. **Daosong Fu:** Resources, Funding acquisition, Conceptualization. **Jingjing Xu:** Writing – review & editing, Validation, Supervision, Project administration, Investigation, Funding acquisition, Conceptualization. **Qun Luo:** Supervision, Project administration, Investigation. **Xiaodong Wu:** Supervision, Project administration, Investigation, Funding acquisition, Conceptualization.

Declaration of competing interest

The authors declare that they have no known competing financial interests or personal relationships that could have appeared to influence the work reported in this paper.

Acknowledgement

This work was financially supported by the National Key R&D Program of China (Grant No.2022YFE0207300), National Natural Science Foundation of China (Grant Nos. 22179142 and 22075314) and Jiangsu Funding Program for Excellent Postdoctoral Talent (Grant No. 2024ZB051 and 2023ZB836). The authors are grateful for the technical support for Nano-X from Suzhou Institute of Nano-Tech and Nano-Bionics, Chinese Academy of Sciences (SINANO).

Appendix A. Supplementary data

Supplementary data to this article can be found online at https://doi.org/10.1016/j.matre.2024.100311.

References

1. Zhang B, Wen W, Wang H, et al. In situ generated of hybrid interface in poly (1, 3-dioxolane) quasi solid electrolyte and extended sulfone cosolvent for lithium-metal batteries. *Chem. Eng. J.* 2023;472:144990.
2. Zhou Q, Zhao H, Fu C, et al. Tailoring electric Double layer by cation specific Adsorption for high-voltage quasi-solid-state lithium metal batteries. *Angew Chem Int Ed.* 2024:e202402625.
3. Liu L, Xue J, Liu Y, et al. Excellent polymerized ionic-liquid-based gel polymer electrolytes enabled by molecular structure design and anion-derived interfacial layer. *ACS Appl Mater Interfaces.* 2024;16(7):8895–8902.
4. Li J, Hu H, Fang W, et al. Impact of fluorine-based lithium salts on SEI for all-solid-state PEO-based lithium metal batteries. *Adv Funct Mater.* 2023;33(38):2303718.
5. Zhou Z, Tao Z, Chen R, et al. Elastomeric electrolyte for high capacity and long-cycle-life solid-state lithium metal battery. *Small Methods.* 2023;7(4):2201328.
6. Wang S, Sun Q, Zhang Q, et al. Li-ion transfer mechanism of ambient-temperature solid polymer electrolyte toward lithium metal battery. *Adv Energy Mater.* 2023;13(16):2204036.
7. Luo L, Sun Z, Gao H, et al. Insights into the enhanced interfacial stability enabled by electronic conductor layers in solid-state Li batteries. *Adv Energy Mater.* 2023;13(10):2203517.
8. Huang Y, Liu S, Chen Q, et al. Constructing highly conductive and thermomechanical stable quasi-solid electrolytes by self-polymerization of liquid electrolytes within porous polyimide nanofiber films. *Adv Funct Mater.* 2022;32(31):2201496.
9. Goujon L, Khaldi A, Maziz A, et al. Flexible solid polymer electrolytes based on nitrile butadiene rubber/poly (ethylene oxide) interpenetrating polymer networks containing either LiTFSI or EMITFSI. *Macromolecules.* 2011;44(24):9683–9691.
10. Fu C, Homann G, Grissa R, et al. A polymerized-ionic-liquid-based polymer electrolyte with high oxidative stability for 4 and 5 V Class solid-state lithium metal batteries. *Adv Energy Mater.* 2022;12(27):2200412.
11. Utomo N, Deng Y, Zhao Q, et al. Structure and evolution of quasi-solid-state hybrid electrolytes formed inside electrochemical cells. *Adv. Mater.* 2022;34(32):2110333.
12. Li Y, Mao E, Min Z, et al. Hybrid polymer-alloy-fluoride interphase enabling fast ion transport kinetics for low-temperature lithium metal batteries. *ACS Nano.* 2023;17(19):19459–19469.
13. Liu Y, Zou H, Huang Z, et al. In situ polymerization of 1, 3-dioxane as a highly compatible polymer electrolyte to enable the stable operation of 4.5 V Li-metal batteries. *Energy Environ Sci.* 2023;16(12):6110–6119.
14. Zhang F, Sun Y, Wang Z, et al. Highly conductive polymeric ionic liquid electrolytes for ambient-temperature solid-state lithium batteries. *ACS Appl Mater Interfaces.* 2020;12(21):23774–23780.
15. Lewis N, Zhang Y, Dereka B, et al. Signatures of ion pairing and aggregation in the vibrational spectroscopy of super-concentrated aqueous lithium bistriflimide solutions. *J Phys Chem C.* 2020;124(6):3470–3481.
16. Noorhisham N, Amri D, Mohamed A, et al. Characterisation techniques for analysis of imidazolium-based ionic liquids and application in polymer preparation: a review. *J Mol Liq.* 2021;326:115340.
17. Ozdemir S, Varlikli C, Oner I, et al. The synthesis of 1, 8-naphthalimide groups containing imidazolium salts/ionic liquids using I^-, PF_6^-, $TFSI^-$ anions and their photophysical, electrochemical and thermal properties. *Dyes Pigments.* 2010;86(3):206–216.
18. Zhao Q, Liu X, Stalin S, et al. Solid-state polymer electrolytes with in-built fast interfacial transport for secondary lithium batteries. *Nat Energy.* 2019;4(5):365–373.
19. Abirami M, Saratha R, Shilpa R, et al. Preparation and characterization of guar gum-based solid biopolymer electrolyte doped with lithium bis (trifluoromethanesulphonyl) imide (LiTFSI) plasticized with glycerol. *B. Mater. Sci.* 2020;43:1–6.
20. Ebadi M, Costa LT, Araujo CM, et al. Modelling the polymer electrolyte/Li-metal interface by molecular dynamics simulations. *Electrochim Acta.* 2017;234:43–51.
21. Bruce P, Evans J, Vincent C. Conductivity and transference number measurements on polymer electrolytes. *Solid State Ionics.* 1988;28:918–922.
22. Du Y, Zhao L, Xiong C, et al. Ameliorating structural and electrochemical properties of traditional poly-dioxolane electrolytes via integrated design of ultra-stable network for solid-state batteries. *Energy Storage Mater.* 2023;56:310–318.
23. Jiang L, Yan C, Yao Y, et al. Inhibiting solvent co-intercalation in a graphite anode by a localized high-concentration electrolyte in fast-charging batteries. *Angew Chem Int Ed.* 2021;60(7):3402–3406.
24. Tang L, Chen B, Zhang Z, et al. Polyfluorinated crosslinker-based solid polymer electrolytes for long-cycling 4.5 V lithium metal batteries. *Nat Commun.* 2023;14(1):2301.
25. Liu F, Wang L, Zhang Z, et al. A mixed lithium-ion conductive Li_2S/Li_2Se protection layer for stable lithium metal anode. *Adv Funct Mater.* 2020;30(23):2001607.
26. Cao X, Ren X, Zou L, et al. Monolithic solid-electrolyte interphases formed in fluorinated orthoformate-based electrolytes minimize Li depletion and pulverization. *Nat Energy.* 2019;4(9):796–805.
27. Yang S, Yuan H, Yao N, et al. Intrinsically safe lithium metal batteries enabled by Thermo-electrochemical compatible in-situ polymerized solid-state electrolytes. *Adv. Mater.* 2024:2405086.

Lingwang Liu is a PhD student at the School of Nano-Tech and Nano-Bionics, University of Science and Technology of China in the group of Prof. Xiaodong Wu. His current research focuses on the structural design of high-performance polymer electrolytes for lithium metal batteries, as well as the investigation into the transport mechanism of lithium ions in solid-state electrolytes.

Jiangyan Xue is a postdoctoral fellow at Suzhou Institute of Nano-Tech and Nano-Bionics (SINANO), Chinese Academy of Sciences (supervisor: Prof. Xiaodong Wu). Her research interests include the development of functional nanomaterials for energy storage and transformation (including water splitting, lithium/sodium ion batteries, and lithium/sodium-sulfur batteries).

Jingjing Xu is currently a professor at the College of Material Science and Engineering, Hohai University. Her research is focused on the fundamental study of electrolytes/ interfaces and key materials for novel energy storage batteries, aiming to address issues such as safety performance and cycle life in the practical application of lithium secondary batteries.

Qun Luo is a researcher in Suzhou Institute of Nano-Tech and Nano-Bionics, Chinese Academy of Sciences. She is mainly engaged in research on inks related to printed organic and perovskite solar cells, large-area transparent conductive electrodes, the construction and application of high-efficiency and large-area flexible batteries.

Xiaodong Wu is a researcher in Suzhou Institute of Nano-Tech and Nano-Bionics, Chinese Academy of Sciences. As the project leader, he has undertaken national key research and development projects, pilot projects of the Chinese Academy of Sciences, general projects of the National Natural Science Foundation of China. His research interests include high-capacity cathode and anode materials for lithium-ion battery, electrolyte/electrode interface and Li-S battery.